Supporting Information

Enhanced Electron-Transfer Reactivity of Nonheme Manganese(IV)-Oxo Complexes by Binding Scandium Ions

Heejung Yoon,[†,‡] Yong-Min Lee,[‡] Xiujuan Wu,[‡] Kyung-Bin Cho,[‡] Ritimukta Sarangi,[§] Wonwoo Nam,[*,‡] and Shunichi Fukuzumi[*,†,‡]

[†]*Department of Material and Life Science, Graduate School of Engineering, ALCA, Japan Science and Technology Agency (JST), Osaka University, Suita, Osaka 565-0871, Japan*

[‡]*Department of Bioinspired Science, Ewha Womans University, Seoul 120-750, Korea*

[§]*Stanford Synchrotron Radiation Lightsource, SLAC National Accelerator Laboratory, Menlo Park, California 94025, United States*

E-mail: fukuzumi@chem.eng.osaka-u.ac.jp, wwnam@ewha.ac.kr

Full reference for Gaussian 09:

Frisch, M. J.; Trucks, G. W.; Schlegel, H. B.; Scuseria, G. E.; Robb, M. A.; Cheeseman, J. R.; Scalmani, G.; Barone, V.; Mennucci, B.; Petersson, G. A.; Nakatsuji, H; Caricato, M.; Li, X.; Hratchian, H. P.; Izmaylov, A. F.; Bloino, J.; Zheng, G.; Sonnenberg, J. L.; Hada, M.; Ehara, M.; Toyota, K.; Fukuda, R.; Hasegawa, J.; Ishida, M.; Nakajima, T.; Honda, Y.; Kitao, O.; Nakai, H.; Vreven, T.; Montgomery, J. A.; Peralta, J. E.; Ogliaro, F.; Bearpark, M.; Heyd, J. J.; Brothers, E.; Kudin, K. N.; Staroverov, V. N.; Kobayashi, R.; Normand, J.; Raghavachari, K.; Rendell, A.; Burant, J. C.; Iyengar, S. S.; Tomasi, J.; Cossi, M.; Rega, N.; Millam, J. M.; Klene, M.; Knox, J. E.; Cross, J. B.; Bakken, V.; Adamo, C.; Jaramillo, J.; Gomperts, R.; Stratmann, R. E.; Yazyev, O.; Austin, A. J.; Cammi, R.; Pomelli, C.; Ochterski, J. W.; Martin, R. L.; Morokuma, K.; Zakrzewski, V. G.; Voth, G. A.; Salvador, P.; Dannenberg, J. J.; Dapprich, S.; Daniels, A. D.; Farkas, Ö.; Foresman, J. B.; Ortiz, J. V.; Cioslowski, J.; Fox, D. J. *Gaussian 09, Revision B.01*, Gaussian Inc.: Wallingford CT, 2009.

Experimental Section for EXAFS Measurements

X-ray Absorption Spectroscopy

The Mn K-edge X-ray absorption spectra of **1**, $[(\text{Bn-TPEN})\text{Mn}^{\text{IV}}(\text{O})]^{2+}$-$(\text{Sc}^{3+})_1$, [herein called $\text{Mn}^{\text{IV}}(\text{O})$-$(\text{Sc}^{3+})_1$] and $[(\text{Bn-TPEN})\text{Mn}^{\text{IV}}(\text{O})]^{2+}$-$(\text{Sc}^{3+})_2$, [herein called $\text{Mn}^{\text{IV}}(\text{O})$-$(\text{Sc}^{3+})_2$] were measured at the Stanford Synchrotron Radiation Lightsource (SSRL) on the unfocussed 20-pole 2 T wiggler side-station beam line 7-3 under standard ring conditions of 3 GeV and ~500 mA. A Si(220) double crystal monochromator was used for energy selection. A Rh-coated harmonic rejection mirror was used on beam line 7-3 to reject components of higher harmonics. The monochromator was further detuned by 70% to eliminate higher harmonic and to reduce beam damage on samples. The solution samples for $\text{Mn}^{\text{IV}}(\text{O})$-$(\text{Sc}^{3+})_1$ and $\text{Mn}^{\text{IV}}(\text{O})$-$(\text{Sc}^{3+})_2$ (~120 μL) were transferred into 2 mm delrin XAS cells with 70 μm Kapton tape windows under synthesis conditions and were immediately frozen after preparation and stored under liquid N_2. During data collection, samples were maintained at a constant temperature of ~10 - 15 K using an Oxford Instruments CF 1208 liquid helium cryostat. Data were measured to k = 12 Å^{-1} (fluorescence mode) using a Canberra Ge 30-element array detector. Internal energy calibration was accomplished by simultaneous measurement of the absorption of a Mn-foil placed between two ionization chambers situated after the sample. The first inflection point of the foil spectrum was fixed at 6539.0 eV. Data presented here are 32-scan average spectra for $\text{Mn}^{\text{IV}}(\text{O})$-$(\text{Sc}^{3+})_1$ and $\text{Mn}^{\text{IV}}(\text{O})$-$(\text{Sc}^{3+})_2$. Data were processed by fitting a second-order polynomial to the pre-edge region and subtracting this from the entire spectrum as background. A four-region spline of orders 2, 3, 3 and 3 was used to model the smoothly decaying post-edge region. The data were normalized by subtracting the cubic spline and assigning the edge jump to 1.0 at 6555 eV using the Pyspline program.[S1] Data were then renormalized in Kaleidagraph for comparison and quantitation purposes.

Theoretical EXAFS signals $\chi(k)$ were calculated by using FEFF (macintosh version 8.4).[S2-S4] Starting structural models for $\text{Mn}^{\text{IV}}(\text{O})$-$(\text{Sc}^{3+})_1$ and $\text{Mn}^{\text{IV}}(\text{O})$-$(\text{Sc}^{3+})_2$. were generated by modifying the crystal structure of $[(\text{Bn-TPEN})\text{Mn}^{\text{II}}(\text{CF}_3\text{SO}_3)]^+$ in Avogadro.[S5] The input structure was improved based on preliminary EXAFS fit parameters to generate more accurate theoretical EXAFS signals. Data fitting was performed in EXAFSPAK.[S6] The structural parameters varied during the fitting process were the bond distance (R) and the bond variance σ^2, which is related to the Debye-Waller factor resulting from thermal motion, and static disorder of the absorbing and scattering atoms. The non-structural parameter E_0 (the energy at which k = 0) was also allowed to vary but was restricted to a common value for

every component in a given fit. Coordination numbers was systematically varied in the course of the fit but were fixed within a given fit.

Results and Analysis

The k^3 weighted Mn K-edge EXAFS data for **1**, $Mn^{IV}(O)$-$(Sc^{3+})_1$ and $Mn^{IV}(O)$-$(Sc^{3+})_2$ along with their non-phase shift corrected Fourier transforms (FT) (k = 1 - 12 $Å^{-1}$) are shown in Figure S3. The EXAFS data for **1** have been previously reported,[S7] but were re-measured under the same experimental conditions for direct comparison to $Mn^{IV}(O)$-$(Sc^{3+})_1$ and $Mn^{IV}(O)$-$(Sc^{3+})_2$. The comparison shows that on going from **1** to $Mn^{IV}(O)$-$(Sc^{3+})_1$ to $Mn^{IV}(O)$-$(Sc^{3+})_2$, the first shell intensity progressively diminishes. In addition, the FT data for $Mn^{IV}(O)$-$(Sc^{3+})_1$ shows a modest increase in intensity at R' ~3 Å relative to $[(Bn\text{-}TPEN)Mn^{IV}(O)]^{2+}$, while a much more intense feature is observed in $Mn^{IV}(O)$-$(Sc^{3+})_2$ at R' ~3 Å.

FEFF fits to the EXAFS data were performed to quantitatively understand the differences visually observed in the FT data. The fits to $Mn^{IV}(O)$-$(Sc^{3+})_1$ and $Mn^{IV}(O)$-$(Sc^{3+})_2$ indicate that the two species have very similar first shells (see Table S1). Both are consistent with a distorted six-coordinate first shell with one short Mn-O (1.74 Å), four Mn-N (~2.07 Å) and a longer Mn-N (2.36 Å in $Mn^{IV}(O)$-$(Sc^{3+})_1$ and 2.27 Å in $Mn^{IV}(O)$-$(Sc^{3+})_2$) distance. This difference in the longer Mn-N bond is likely due to an increase in error associated with a strong correlation of the weaker Mn-N parameters with those of the short Mn-N component. The second and third EXAFS shells were fit with single and multiple scattering components from the Bn-TPEN ligand system. The intense peak at ~3 Å observed for $Mn^{IV}(O)$-$(Sc^{3+})_2$ was fit with a Mn-Sc interaction at ~3.44 Å. Both single (Mn-Sc at 3.44 Å) and multiple scattering (Mn-O-Sc at 3.52 Å) components were required to obtain a good fit. In $Mn^{IV}(O)$-$(Sc^{3+})_1$, this feature is less obvious and the increase in goodness of fit upon the inclusion of the corresponding Mn-Sc parameters was small. The single and multiple scattering components optimized to 3.45 and 3.59 Å, respectively. The larger difference between the single and multiple scattering components in $Mn^{IV}(O)$-$(Sc^{3+})_1$ (0.14 Å) compared to $Mn^{IV}(O)$-$(Sc^{3+})_2$ (0.08 Å), indicates that the Mn-O-Sc angle is steeper in $Mn^{IV}(O)$-$(Sc^{3+})_1$ relative to $Mn^{IV}(O)$-$(Sc^{3+})_2$. This is consistent with the weaker intensity at 3 Å, since intense multiple scattering components would only contribute strongly if the Mn-O-Sc were close to linearity.

The EXAFS fit results show that upon Sc^{3+} binding, the Mn=O distance increases from 1.69 in **1** to 1.74 Å in both $Mn^{IV}(O)$-$(Sc^{3+})_1$ and $Mn^{IV}(O)$-$(Sc^{3+})_2$. This is in excellent

agreement with DFT results, which show that the Mn=O in **1**, $Mn^{IV}(O)$-$(Sc^{3+})_1$ and $Mn^{IV}(O)$-$(Sc^{3+})_2$ are 1.68 Å, 1.75 Å and 1.75 Å, respectively. The Mn-Sc distance from the DFT is somewhat longer than that predicted by the EXAFS results for both $Mn^{IV}(O)$-$(Sc^{3+})_1$ and $Mn^{IV}(O)$-$(Sc^{3+})_2$ (by ~0.2 Å). Similar discrepancy has been observed in previous studies, where DFT calculated metal-metal distances was predicted to be longer than the EXAFS distances.[S8,S9] This difference is likely attributed to a combination of higher EXAFS error at longer distances (~ 0.1 Å) and shortcomings in DFT to accurately predict the metal-metal distance. In one study, this difference has been attributed to a flat potential energy surface along the metal-metal distance coordinate.[S9] Interestingly, the Mn-O-Sc angle in $Mn^{IV}(O)$-$(Sc^{3+})_1$ is 162.9°, while that in $Mn^{IV}(O)$-$(Sc^{3+})_2$ is 170.6°. The steeper calculated Mn-O-Sc angle in $Mn^{IV}(O)$-$(Sc^{3+})_1$ is consistent with the EXAFS results and supports the theory that the non-linear Mn-O-Sc in $Mn^{IV}(O)$-$(Sc^{3+})_1$ results in a weaker EXAFS signal at ~ 3 Å.

References

(S1) Tenderholt, A.; Hedman, B.; Hodgson, K. O. *PySpline: A Modern, Cross-Platform Program for the Processing of Raw Averaged XAS Edge and EXAFS Data; X-ray Absorption Fine Structure - XAFS13*, **2007**, *882*, 105-107.

(S2) Zabinsky, S. I.; Rehr, J. J.; Ankudinov, A.; Albers, R. C.; Eller, M. J. *Phys. Rev. B: Condens. Matter* **1995**, *52*, 2995-3009.

(S3) Mustre de Leon, J.; Rehr, J. J.; Zabinsky, S. I.; Albers, R. C. *Phys. Rev. B: Condens. Matter* **1991**, *44*, 4146-4156.

(S4) Rehr, J. J.; Mustre de Leon, J.; Zabinsky, S. I.; Albers, R. C. *J. Am. Chem. Soc.* **1991**, *113*, 5135-5140.

(S5) Avogadro: an open-source molecular builder and visualization tool. Version 1.1.0. http://avogadro.openmolecules.net/.

(S6) George, G. N. *EXAFSPAK and EDG-FIT*, Stanford Synchrotron Radiation Laboratory, Stanford Linear Accelerator Center, Stanford, CA, 2000.

(S7) Wu, X.; Seo, M. S.; Davis, K. M.; Lee, Y. M.; Chen, J.; Cho, K. B.; Pushkar, Y. N.; Nam, W. *J. Am. Chem. Soc.* **2011**, *133*, 20088-20091.

(S8) Chen, J.; Lee, Y. M.; Davis, K. M.; Wu, X.; Seo, M. S.; Cho, K. B.; Yoon, H.; Park, Y. J.; Fukuzumi, S.; Pushkar, Y. N.; Nam, W. *J. Am. Chem. Soc.* **2013**, *135*, 6388-6391.

(S9) Del Rio, D.; Sarangi, R.; Chufan, E. E.; Karlin, K. D.; Hedman, B.; Hodgson, K. O.; Solomon, E. I. *J. Am. Chem. Soc.* **2005**, *127*, 11969-11978.

Table S1. EXAFS Least Squares Fitting Results

Complex	Coordination/Path	R(Å)[a]	σ^2(Å^2)[b]	E_0 (eV)	F[c]
$Mn^{IV}(O)$-$(Sc^{3+})_1$	1 Mn-O	1.74	640	-3.26	0.42
	4 Mn-N	2.07	575		
	1 Mn-N	2.36	95		
	6 Mn-C	2.94	334		
	12 Mn-C-N	3.32	/334		
	1 Mn-Sc[d]	3.45	160		
	2 Mn-O-Sc[d]	3.59	461		
	4 Mn-C-N	4.37	597		
$Mn^{IV}(O)$-$(Sc^{3+})_2$	1 Mn-O	1.74	841	-3.78	0.36
	4 Mn-N	2.08	838		
	1 Mn-N	2.27	358		
	6 Mn-C	2.91	410		
	12 Mn-C-N	3.35	/410		
	1 Mn-Sc[d]	3.44	140		
	2 Mn-O-Sc[d]	3.52	139		
	4 Mn-C-N	4.26	619		

[a]The estimated standard deviations for the distances are in the order of ± 0.02 Å. [b]The σ^2 values are multiplied by 10^5. [c]Error is given by $\Sigma[(\chi_{obsd} - \chi_{calcd})^2 k^6]/\Sigma[(\chi_{obsd})^2 k^6]$. [d]/ indicates the σ^2 value for the path is linked to the preceding path. The S_0^2 factor was set at 0.95.

Table S2. Selected Geometries in Å

species	Mn-O	MnO-Sc_A	MnO-Sc_B	Sc_A-Sc_B	Mn-Sc_A	Mn-Sc_B
[(Bn-TPEN)Mn^{IV}O][a]	1.68	---	---	---	---	---
[(Bn-TPEN)Mn^{IV}O]-$(Sc^{3+})_1$	1.75	1.94	---	---	3.65	---
[(Bn-TPEN)Mn^{IV}O]-$(Sc^{3+})_2$	1.75	1.94	6.11	5.35	3.68	7.09

[a] Values taken from ref 41a in the text.

Table S3. Mulliken Spin Density Distribution

species	Mn	O	Sc_A	Sc_B	5 x N	rest of Bn-TPEN	6 x OTf
[(Bn-TPEN)Mn^{IV}O][a]	2.64	0.63	---	---	-0.15	0.02	---
[(Bn-TPEN)Mn^{IV}O]-$(Sc^{3+})_1$	3.13	0.27	0.02	---	-0.50	0.06	0.02[b]
[(Bn-TPEN)Mn^{IV}O]-$(Sc^{3+})_2$	3.14	0.29	0.01	0.00	-0.54	0.08	0.03

[a] Values taken from ref 41a in the main text. [b] 3 x OTf.

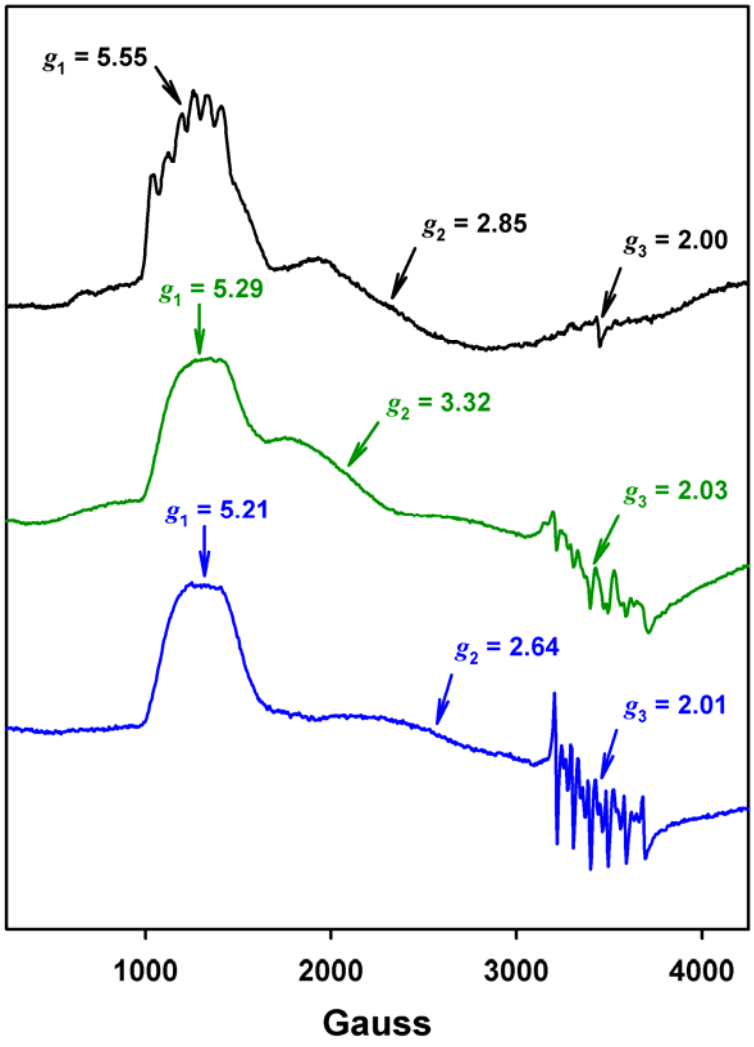

Figure S1. X-band CW-EPR spectra of $[(\text{Bn-TPEN})\text{Mn}^{\text{IV}}(\text{O})]^{2+}$ (1.0 mM, black line), $[(\text{Bn-TPEN})\text{Mn}^{\text{IV}}(\text{O})]^{2+}$–$(\text{Sc}^{3+})_1$ (1.0 mM, green line), and $[(\text{Bn-TPEN})\text{Mn}^{\text{IV}}(\text{O})]^{2+}$–$(\text{Sc}^{3+})_2$ (1.0 mM, blue line). Spectra were recorded in $\text{CF}_3\text{CH}_2\text{OH}/\text{CH}_3\text{CN}$ (v/v = 19:1) at 5 K.

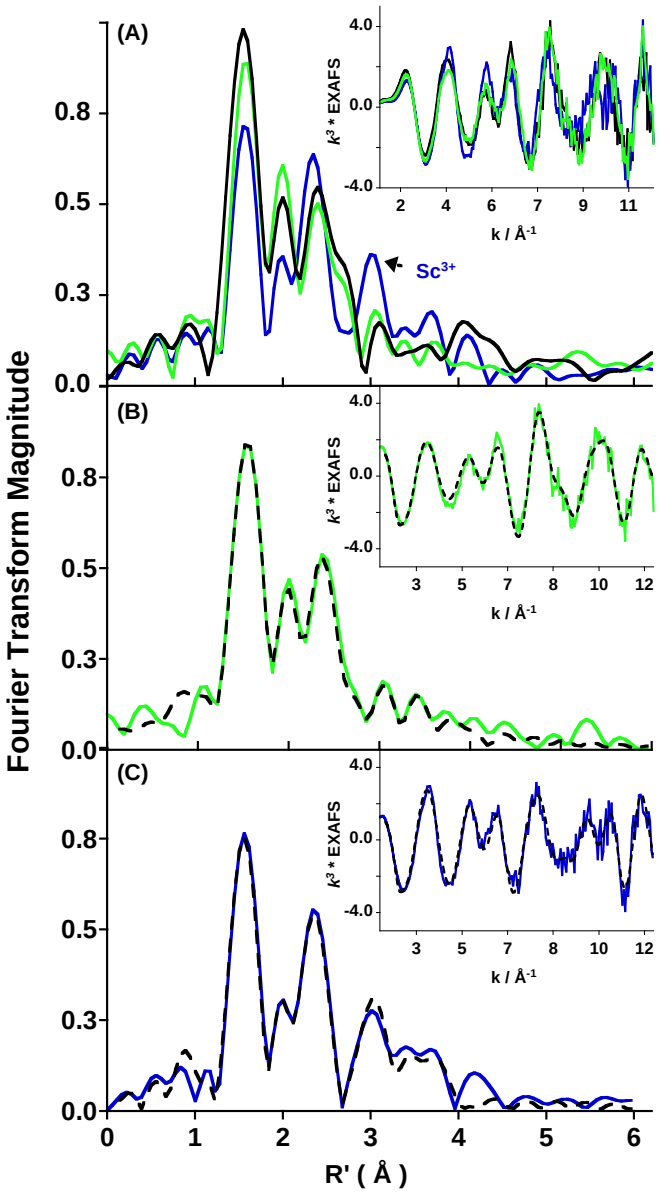

Figure S2. (A) A comparison of the non phase-shift corrected Fourier transforms and the corresponding Mn K-edge EXAFS data (inset) for **1** (—), $Mn^{IV}(O)$-$(Sc^{3+})_1$ (—) and $Mn^{IV}(O)$-$(Sc^{3+})_2$ (—). FEFF best-fits (- - -) to $Mn^{IV}(O)$-$(Sc^{3+})_1$ (—) and $Mn^{IV}(O)$-$(Sc^{3+})_2$ (—) are shown in (B) and (C), respectively. Fits were performed over k = 2 - 12 $Å^{-1}$ range.

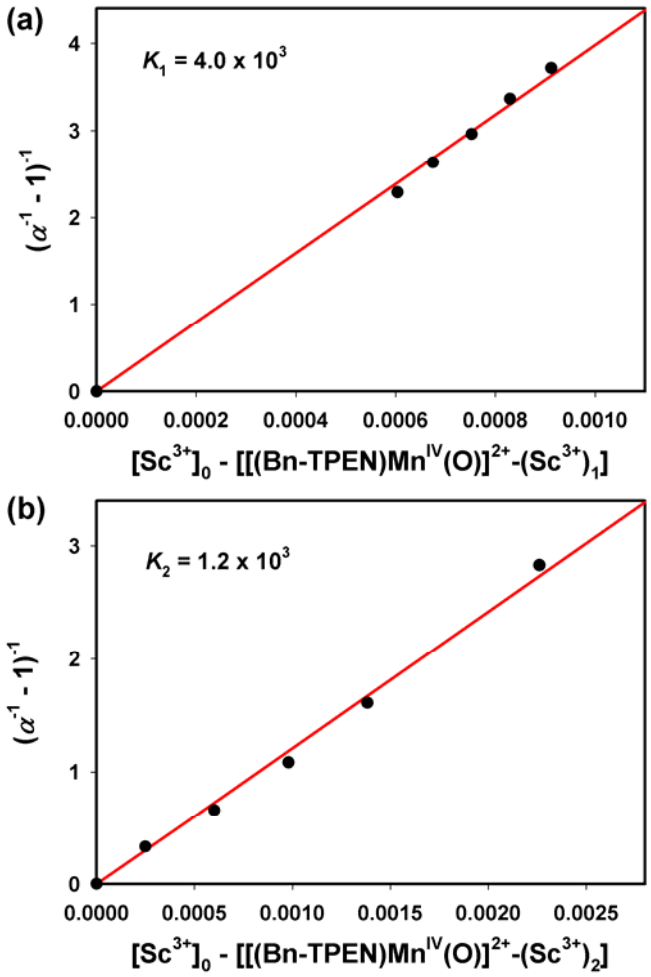

Figure S3. (a) Plot of $(\alpha^{-1} - 1)^{-1}$ vs $[Sc^{3+}]_0 - [[(BnTPEN)Mn^{IV}(O)]^{2+}\text{-}(Sc^{3+})_1]$ to determine the first binding constant ($K_1 = [[Mn^{IV}(O)]^{2+}\text{-}(Sc^{3+})_1]/[[Mn^{IV}(O)]^{2+}][Sc^{3+}]$) upon addition of Sc^{3+} (0.0 – 2.0 mM) into the solution of $[(BnTPEN)Mn^{IV}(O)]^{2+}$ (1.0 mM) in CF_3CH_2OH/CH_3CN (v/v = 1:1) at 298 K; $\alpha = [[(BnTPEN)Mn^{IV}(O)]^{2+}\text{-}(Sc^{3+})_1]/[[(BnTPEN)Mn^{IV}(O)]^{2+}]_0$. (b) Plot of $(\alpha^{-1} - 1)^{-1}$ vs $[Sc^{3+}]_0 - [[(BnTPEN)Mn^{IV}(O)]^{2+}\text{-}(Sc^{3+})_2]$ to determine the second binding constant ($K_2 = [[Mn^{IV}(O)]^{2+}\text{-}(Sc^{3+})_2]/[[Mn^{IV}(O)]^{2+}\text{-}(Sc^{3+})_1][Sc^{3+}]$) upon addition of Sc^{3+} (0.0 – 12 mM) into the solution of $[(BnTPEN)Mn^{IV}(O)]^{2+}\text{-}(Sc^{3+})_1$ (1.0 mM) in CF_3CH_2OH/CH_3CN (v/v = 1:1) at 298 K; $\alpha = [[(BnTPEN)Mn^{IV}(O)]^{2+}\text{-}(Sc^{3+})_2]/[[(BnTPEN)Mn^{IV}(O)]^{2+}\text{-}(Sc^{3+})_1]_0$. The expression used for the determination of K_1 and K_2 was derived according to ref 43 in the text.

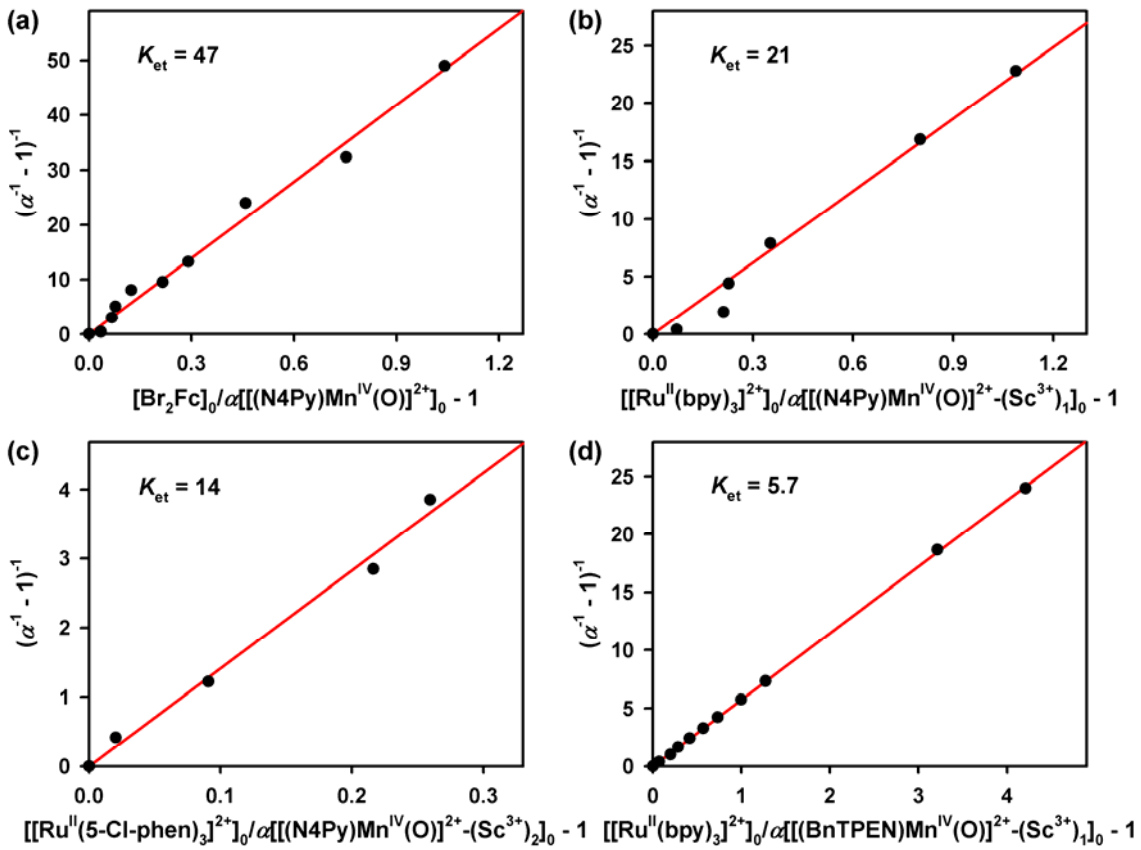

Figure S4. (a) Plot of $(\alpha^{-1} - 1)^{-1}$ vs $[Br_2Fc]_0/\alpha[[(N4Py)Mn^{IV}(O)]^{2+}]_0 - 1$ to determine equilibrium constants ($K_{et} = [Br_2Fc^+][[Mn^{III}(O)]^+]/[Br_2Fc][[Mn^{IV}(O)]^{2+}]$) for electron transfer from Br_2Fc to $[(N4Py)Mn^{IV}(O)]^{2+}$ upon addition of Br_2Fc (0.0 – 2.5 mM) into the solution of $[(N4Py)Mn^{IV}(O)]^{2+}$ (0.50 mM) in CF_3CH_2OH/CH_3CN (v/v = 1:1) at 273 K ($\alpha = [Br_2Fc^+]/[[(N4Py)Mn^{IV}(O)]^{2+}]_0$). The slope of the linear plot corresponds to K_{et}. The linear correlation can be derived from the electron-transfer equilibrium in eq 1. The same analyses were performed to determine the K_{et} values for $(N4Py)Mn^{IV}(O)]^{2+}\text{-}(Sc^{3+})_1$ (b), $[(N4Py)Mn^{IV}(O)]^{2+}\text{-}(Sc^{3+})_2$ (c), and $(Bn\text{-}TPEN)Mn^{IV}(O)]^{2+}\text{-}(Sc^{3+})_1$ (d).

(b) Plot of $(\alpha^{-1} - 1)^{-1}$ vs $[[Ru^{II}(bpy)_3]^{2+}]_0/\alpha[[(N4Py)Mn^{IV}(O)]^{2+}\text{-}(Sc^{3+})_1]_0 - 1$ ($\alpha = [[Ru^{III}(bpy)_3]^{3+}]/[[(N4Py)Mn^{IV}(O)]^{2+}\text{-}(Sc^{3+})_1]_0$).

(c) Plot of $(\alpha^{-1} - 1)^{-1}$ vs $[[Ru^{II}(5\text{-Cl-phen})_3]^{2+}]_0/\alpha[[(N4Py)Mn^{IV}(O)]^{2+}\text{-}(Sc^{3+})_2]_0 - 1$ ($\alpha = [[Ru^{III}(5\text{-Cl-phen})_3]^{3+}]/[[(N4Py)Mn^{IV}(O)]^{2+}\text{-}(Sc^{3+})_2]_0$).

(d) Plot of $(\alpha^{-1} - 1)^{-1}$ vs $[[Ru^{II}(bpy)_3]^{2+}]_0/\alpha[[(BnTPEN)Mn^{IV}(O)]^{2+}\text{-}(Sc^{3+})_1]_0 - 1$ ($\alpha = [[Ru^{III}(bpy)_3]^{3+}]/[[(BnTPEN)Mn^{IV}(O)]^{2+}\text{-}(Sc^{3+})_1]_0$.

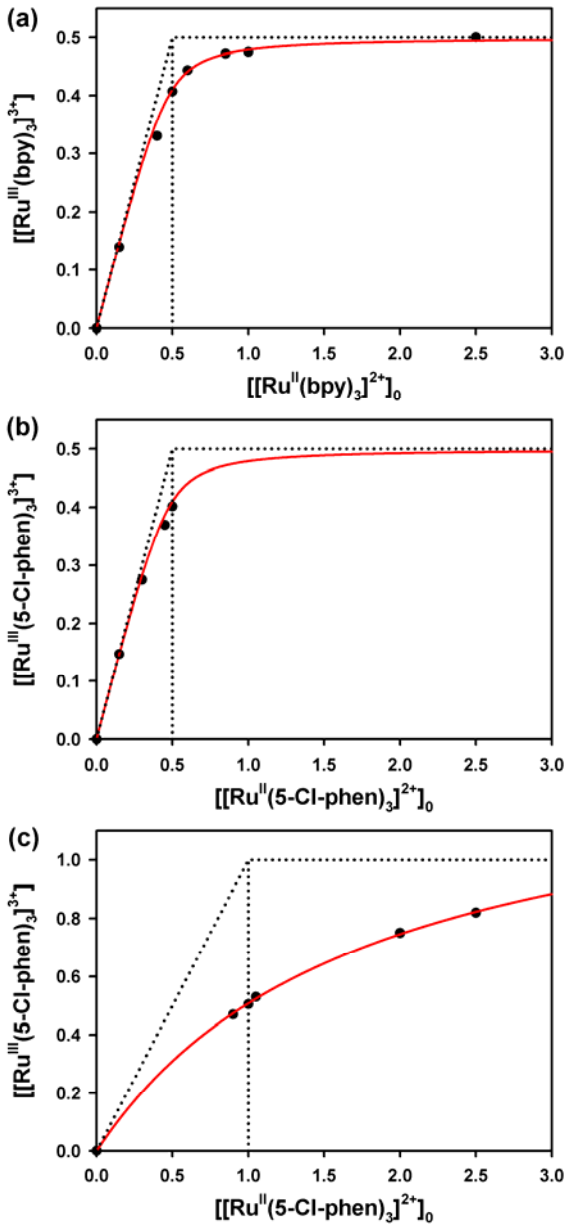

Figure S5. (a) Plot of concentration of $[Ru^{III}(bpy)_3]^{3+}$ produced in electron transfer from $[Ru^{II}(bpy)_3]^{2+}$ (1.24 V vs SCE) to $[(N4Py)Mn^{IV}(O)]^{2+}$-$(Sc^{3+})_1$ vs initial concentration of $[Ru^{II}(bpy)_3]^{2+}$ in CF_3CH_2OH/CH_3CN (v/v = 1:1) at 273 K. (b) Plot of concentration of $[Ru^{III}(5\text{-Cl-phen})_3]^{3+}$ produced in electron transfer from $[Ru^{II}(5\text{-Cl-pehn})_3]^{2+}$ (1.36 V vs SCE) to $[(N4Py)Mn^{IV}(O)]^{2+}$-$(Sc^{3+})_2$ vs initial concentration of $[Ru^{II}(5\text{-Cl-phen})_3]^{2+}$ in CF_3CH_2OH/CH_3CN (v/v = 1:1) at 273 K. (c) Plot of concentration of $[Ru^{III}(5\text{-Cl-phen})_3]^{3+}$ produced in electron transfer from $[Ru^{II}(5\text{-Cl-phen})_3]^{2+}$ to $[(Bn\text{-TPEN})Mn^{IV}(O)]^{2+}$-$(Sc^{3+})_2$ vs initial concentration of $[Ru^{II}(5\text{-Cl-phen})_3]^{2+}$ in CF_3CH_2OH/CH_3CN (v/v = 1:1) at 273 K.

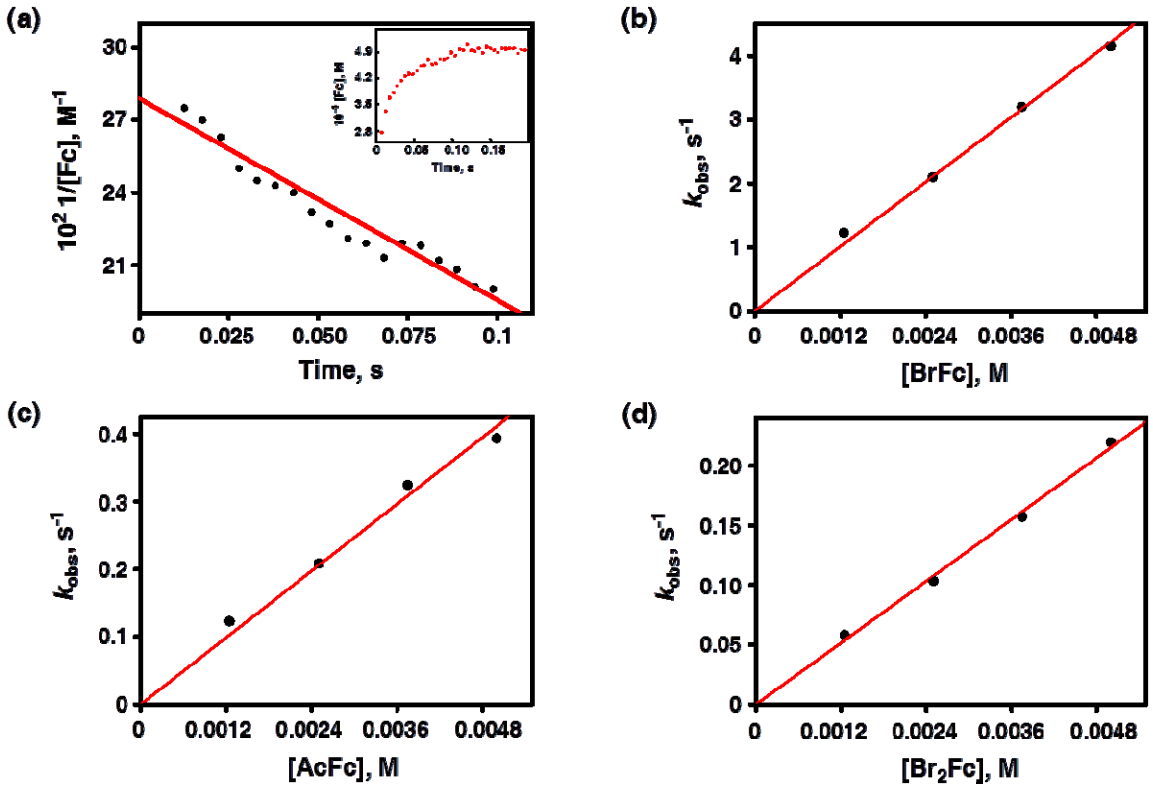

Figure S6. (a) Second-order-plot of 1/[Fc] vs time for electron transfer from ferrocene (5.0×10^{-4} M) to $[(N4Py)Mn^{IV}(O)]^{2+}$ (5.0×10^{-4} M). Inset shows time course of the absorbance change monitored at 615 nm due to ferrocenium ion (ε_{615} = 400 M^{-1} cm^{-1}). (b, c, d) Plots of pseudo-first-order rate constant (k_{obs}) vs concentrations of ferrocene derivatives to determine the second-order rate constants of electron transfer from ferrocene derivatives [(b) bromoferrocene (BrFc), (c) acetylferrocene (AcFc), and (d) dibromoferrocene (Br_2Fc)] to $[(N4Py)Mn^{IV}(O)]^{2+}$ (1.25×10^{-4} M) in CF_3CH_2OH/CH_3CN (v/v = 1:1) at 273 K.

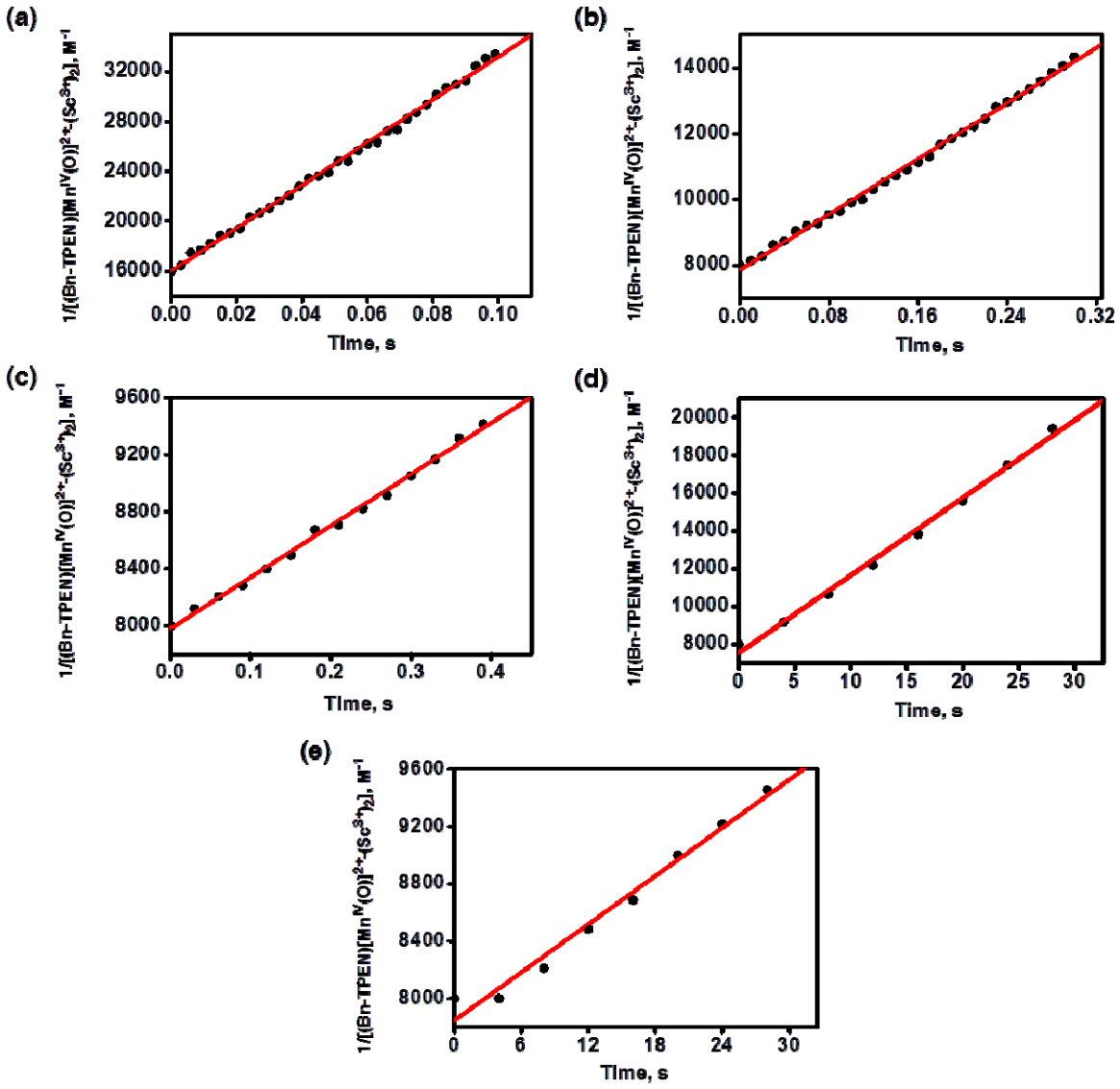

Figure S7. Second-order-plots of $1/[[(Bn\text{-}TPEN)Mn^{IV}(O)]^{2+}\text{-}(Sc^{3+})_2]$ vs time for electron transfer from one-electron reductants (1.25×10^{-5} M; (a) $[Fe^{II}(Me_2\text{-}bpy)_3]^{2+}$, (b) $[Fe^{II}(Ph_2\text{-}phen)_3]^{2+}$, (c) $[Fe^{II}(bpy)_3]^{2+}$, (d) $[Fe^{II}(5\text{-}Cl\text{-}phen)_3]^{2+}$, and (e) $[Ru^{II}(bpy)_3]^{2+}$) to $[(Bn\text{-}TPEN)Mn^{IV}(O)]^{2+}\text{-}(Sc^{3+})_2$ (1.25×10^{-5} M) in CF_3CH_2OH/CH_3CN (v/v = 1:1) at 273 K.

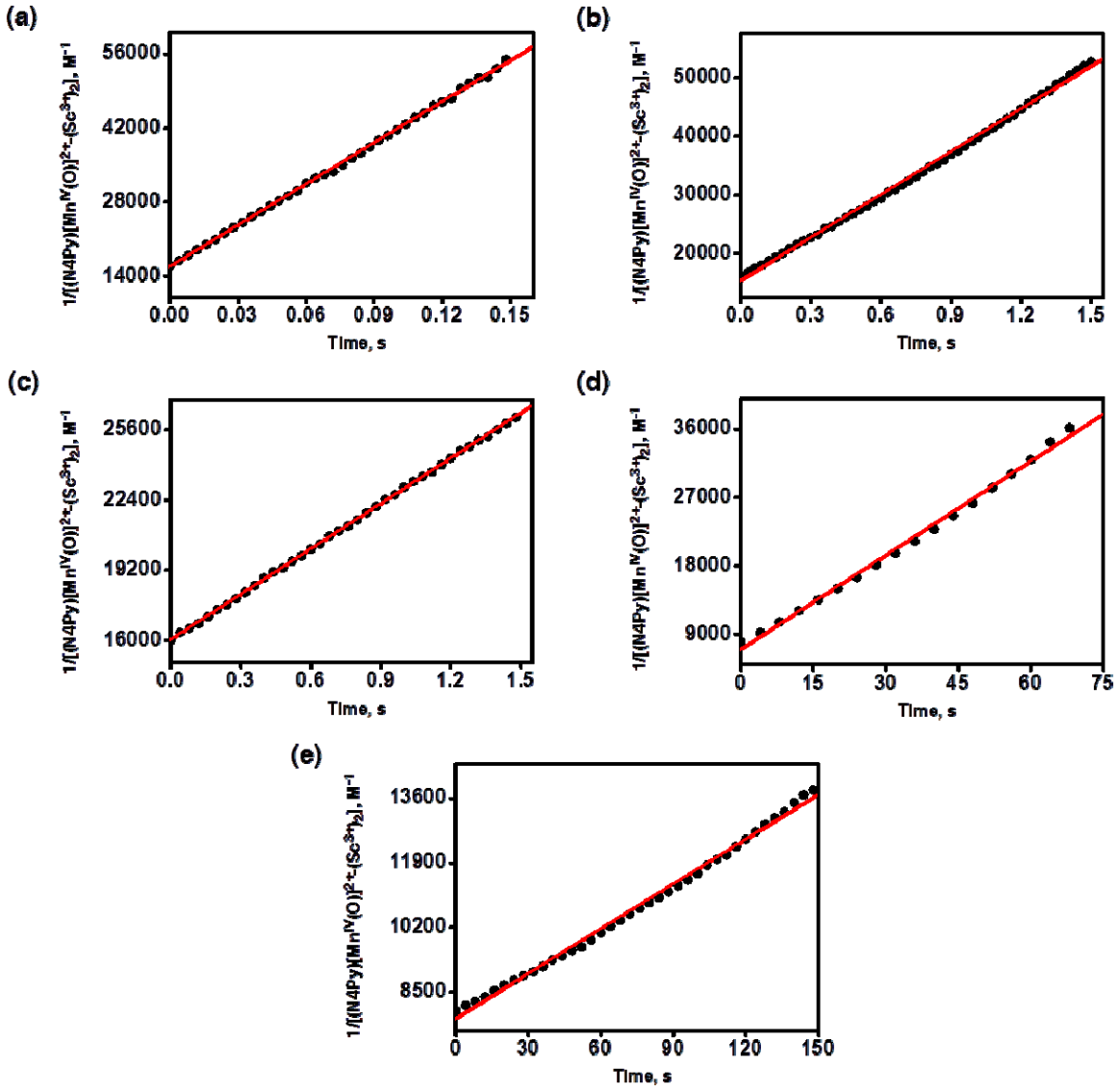

Figure S8. Second-order-plots of 1/[[(N4Py)Mn^{IV}(O)]$^{2+}$-(Sc^{3+})$_2$] vs time for electron transfer from one-electron reductants (1.25 × 10^{-5} M; (a) [Fe^{II}(Me_2-bpy)$_3$]$^{2+}$, (b) [Fe^{II}(Ph_2-phen)$_3$]$^{2+}$, (c) [Fe^{II}(bpy)$_3$]$^{2+}$, (d) [Fe^{II}(5-Cl-phen)$_3$]$^{2+}$, and (e) [Ru^{II}(bpy)$_3$]$^{2+}$) to [(N4Py)Mn^{IV}(O)]$^{2+}$-(Sc^{3+})$_2$ (1.25 × 10^{-5} M) in CF_3CH_2OH/CH_3CN (v/v = 1:1) at 273 K.

DFT Calculated Coordinates

The coordinates are given in xyz-file format and (charge/multiplicity) is given in the comment field.

```
63
(BnTPEN)MnO from ref 41a (2/4)
Mn 7.53277 10.19064 3.40733
N 8.36706 11.96077 2.98090
N 6.52409 10.90759 5.00706
N 5.89003 11.19833 2.41873
N 6.39951 8.45918 3.08135
N 8.55303 9.33636 1.79415
C 9.44562 12.47468 3.62055
H 9.84321 11.88280 4.43331
C 9.99867 13.69052 3.22371
H 10.85943 14.08488 3.74737
C 9.42674 14.37724 2.14653
H 9.83986 15.32363 1.81914
C 8.30846 13.83969 1.49510
H 7.84291 14.35975 0.66754
C 7.78878 12.62258 1.92930
C 6.58468 11.94017 1.31379
H 5.91933 12.66831 0.83760
H 6.89034 11.22040 0.54794
C 5.25675 12.17819 3.37271
H 4.19520 12.30768 3.14128
H 5.72902 13.15661 3.23708
C 5.46913 11.74137 4.79211
C 4.69871 12.21190 5.85649
H 3.85529 12.86246 5.66153
C 5.03698 11.84089 7.16069
H 4.44926 12.19781 7.99788
C 6.14397 11.00921 7.37215
H 6.44009 10.71073 8.36931
C 6.86873 10.55633 6.27543
H 7.73283 9.91226 6.36018
C 4.89170 10.15140 1.98897
H 4.42080 10.43248 1.04059
H 4.10395 10.13111 2.74463
C 5.54505 8.78259 1.86224
H 4.78463 8.00644 1.73198
H 6.19431 8.75066 0.98712
C 7.41789 7.40763 2.72475
H 6.92700 6.51654 2.32414
H 7.93910 7.13434 3.64698
C 8.39766 7.98203 1.74612
C 9.13636 7.19599 0.86272
H 8.97821 6.12505 0.83909
C 10.07198 7.80573 0.02248
H 10.65840 7.21074 -0.66693
C 10.23531 9.19275 0.08392
H 10.94798 9.70515 -0.54894
C 9.46259 9.92854 0.97845
H 9.57534 10.99811 1.05041
C 5.57071 8.01836 4.29377
H 4.87215 8.82708 4.51038
H 6.27929 7.95329 5.12175
C 4.82031 6.71206 4.12711
C 3.49098 6.70364 3.66441
H 2.99077 7.63989 3.43472
C 2.79182 5.49955 3.52223
H 1.76743 5.51070 3.16539
C 3.40966 4.28682 3.85086
H 2.86739 3.35328 3.74395
C 4.72492 4.28411 4.33264
H 5.20306 3.34939 4.60570
C 5.42354 5.48809 4.47314
H 6.43561 5.47575 4.86666
O 8.70688 9.54045 4.41067

88
Mn(IV)O-Sc(3+) (2/4)
Mn -0.46899 -0.12280 0.76650
N -1.63046 -1.68010 1.29869
N -0.93398 -0.28933 -1.18709
N -2.38476 0.75229 0.77987
N 0.21109 1.86202 0.73771
N 0.11745 0.12893 2.74668
C -1.33229 -2.98802 1.09853
H -0.42843 -3.21467 0.55423
C -2.17381 -3.99044 1.57580
H -1.90992 -5.02598 1.41068
C -3.33555 -3.63580 2.26850
H -4.00019 -4.40037 2.65090
C -3.64806 -2.28108 2.45035
H -4.55587 -1.98077 2.95768
C -2.78374 -1.31346 1.95064
C -3.02446 0.17448 2.01995
H -4.09271 0.40984 2.04560
H -2.56091 0.62578 2.90119
C -3.16150 0.29865 -0.44157
H -3.89631 1.06133 -0.71221
H -3.71922 -0.60774 -0.19087
C -2.21585 -0.00213 -1.55908
C -2.60576 -0.07349 -2.89455
H -3.62420 0.17123 -3.16775
C -1.67453 -0.47300 -3.85815
H -1.96388 -0.53803 -4.89978
C -0.37029 -0.79108 -3.46119
H 0.37795 -1.11994 -4.16917
C -0.02516 -0.68636 -2.11932
H 0.96553 -0.91396 -1.76228
C -2.25222 2.26301 0.76590
H -3.08104 2.71383 1.31988
H -2.34130 2.58134 -0.27349
C -0.92150 2.68241 1.34935
H -0.73208 3.74341 1.16351
H -0.89885 2.52945 2.42827
C 1.39281 1.89426 1.67235
H 1.64590 2.93029 1.91340
H 2.24755 1.44906 1.15817
C 1.06019 1.10805 2.90218
C 1.69477 1.31322 4.12446
H 2.42380 2.10770 4.21919
C 1.38204 0.48548 5.20713
H 1.86877 0.62945 6.16368
C 0.43672 -0.52937 5.03407
H 0.17309 -1.20010 5.84068
C -0.17643 -0.68701 3.79456
H -0.89017 -1.47772 3.63769
C 0.61358 2.34358 -0.67209
H -0.27548 2.25796 -1.29602
H 1.35214 1.62137 -1.02423
C 1.16095 3.75433 -0.73157
C 0.30172 4.83578 -1.00505
H -0.75560 4.65925 -1.17877
C 0.80169 6.13977 -1.08637
H 0.12786 6.96220 -1.30049
C 2.16938 6.37837 -0.90400
H 2.55848 7.38878 -0.96945
C 3.03607 5.30743 -0.65166
H 4.09883 5.48450 -0.52671
C 2.53717 4.00308 -0.57003
H 3.22436 3.18256 -0.39276
O 1.06720 -0.91501 0.50492
O 2.40501 -2.65156 -3.35010
S 2.97283 -3.56093 -2.34591
C 1.70561 -4.91636 -2.12522
F 1.49384 -5.55778 -3.32694
O 2.94217 -2.95465 -0.94080
Sc 2.69239 -1.94889 0.76500
O 3.04149 -4.45674 4.13313
S 1.88278 -4.28315 3.25130
C 1.67218 -5.91166 2.35927
F 0.66519 -5.82189 1.41517
O 2.18966 -3.38385 2.04900
O 4.15148 -0.81113 1.53113
S 5.52241 -0.36954 2.05813
O 6.57991 -1.34145 1.76133
O 5.43618 0.20865 3.40341
C 5.82835 1.07227 0.91117
F 5.79927 0.66846 -0.40702
O 4.23889 -4.24176 -2.63259
O 0.57149 -3.98235 3.83981
F 0.50075 -4.38691 -1.69580
F 2.13042 -5.84316 -1.19826
F 2.83833 -6.27592 1.72237
F 1.33501 -6.89677 3.26327
F 7.05973 1.63067 1.17517
F 4.86105 2.04847 1.08935

113
Mn(IV)O-2xSc(3+) (2/4)
Mn -0.36421 0.27846 1.09492
N -0.97817 0.58039 -0.79497
N 0.46503 2.11241 1.25951
N -2.10085 1.43260 1.37993
N -0.53773 -0.13673 3.13812
N -1.17379 -1.63734 1.04692
C -0.17261 0.56974 -1.88594
H 0.88494 0.44502 -1.71158
C -0.70391 0.71872 -3.16571
H -0.04167 0.71305 -4.02215
C -2.08662 0.87470 -3.31308
H -2.52198 0.98677 -4.29837
C -2.90936 0.90855 -2.17791
H -3.97759 1.05944 -2.26720
C -2.33373 0.76781 -0.92014
C -3.08182 0.85201 0.38865
H -3.96553 1.49143 0.30687
H -3.41006 -0.12858 0.74385
C -1.81920 2.87566 1.00581
H -2.48984 3.53470 1.56395
H -2.04273 3.01711 -0.05534
C -0.37808 3.18673 1.24863
C 0.11206 4.48428 1.38075
H -0.57683 5.31912 1.38121
C 1.48972 4.68480 1.50102
H 1.88763 5.68699 1.60106
C 2.34645 3.57796 1.49247
H 3.41696 3.69273 1.58763
C 1.80894 2.30161 1.37390
H 2.42608 1.41741 1.37754
C -2.52073 1.35589 2.83537
H -3.61021 1.42313 2.91214
H -2.10375 2.23147 3.33491
C -2.01447 0.07536 3.46294
H -2.14130 0.09340 4.54874
H -2.56347 -0.78693 3.08535
C -0.21481 -1.60392 3.27431
H -0.51770 -1.95966 4.26203
H 0.86575 -1.72875 3.19119
C -0.90960 -2.35279 2.18135
C -1.25116 -3.69958 2.28290
H -1.03603 -4.23339 3.19868
C -1.85233 -4.33780 1.19507
H -2.12316 -5.38443 1.25665
C -2.09735 -3.60642 0.02908
H -2.55536 -4.06334 -0.83772
C -1.74340 -2.26194 -0.01877
H -1.91382 -1.68414 -0.91138
C 0.40506 0.71239 4.01675
H 0.09236 1.74928 3.89734
H 1.39575 0.59466 3.57608
C 0.42986 0.32493 5.47978
C -0.45886 0.91434 6.39909
H -1.16654 1.66967 6.07030
C -0.41719 0.56185 7.75265
H -1.10679 1.02482 8.45017
C 0.52032 -0.37437 8.20574
H 0.55358 -0.64554 9.25553
C 1.42750 -0.94536 7.30388
H 2.17138 -1.65296 7.65414
C 1.38646 -0.59594 5.94982
H 2.11590 -1.01838 5.26510
O 1.20109 -0.45410 0.82759
Sc 3.11438 -1.01096 -4.94919
O 3.96096 0.67298 -6.33131
S 2.62944 1.37146 -6.47240
C 2.78023 2.97253 -5.50761
F 3.28379 2.73006 -4.25045
O 4.38314 -0.21550 -3.55239
S 4.83839 0.03202 -2.13288
C 6.48875 -0.85234 -2.10414
F 7.31869 -0.30373 -3.05200
O 2.45680 -2.34937 -3.59556
S 2.18761 -3.36956 -2.51348
C 0.48801 -3.98307 -2.99484
F 0.55237 -4.55552 -4.24353
O 2.98000 -2.17837 -6.50498
S 2.91906 -3.32343 -7.53815
O 1.75277 -3.19156 -8.41436
O 1.71142 0.50773 -5.58932
O 1.94648 -2.69274 -1.20241
Sc 2.77988 -1.48935 0.37031
O 4.19429 -4.39361 3.06985
S 2.81767 -4.22977 2.58978
C 2.51620 -5.67843 1.44676
F 1.29546 -5.56030 0.80951
O 4.00700 -0.76216 -1.17981
O 2.66290 -3.07460 1.60229
O 4.04934 -0.54099 1.65999
S 5.09574 -0.59158 2.77459
O 6.22788 -1.47311 2.46328
O 4.48659 -0.66160 4.11116
C 5.77896 1.14023 2.63849
F 6.30880 1.37289 1.38668
O 3.08605 -4.51630 -2.51661
O 1.71796 -4.26092 3.56552
O 5.07202 1.43044 -1.80029
O 2.13915 1.73464 -7.79341
C 4.40465 -2.86104 -8.57586
F 4.58684 -3.80524 -9.56305
O 3.23351 -4.62026 -6.93367
F 7.05987 -0.71015 -0.86200
F 6.31543 -2.19084 -2.37234
F -0.41208 -2.94162 -3.02342
F 0.06441 -4.92267 -2.08560
F 3.50383 -5.75569 0.48566
F 2.51740 -6.85135 2.17356
F 6.77716 1.31677 3.57548
F 4.79216 2.08142 2.87693
F 3.62500 3.82654 -6.17526
F 1.54080 3.55587 -5.39215
F 5.54125 -2.81253 -7.79441
F 4.22328 -1.62963 -9.16766
```